China SV2 (SuperView Neo-2) X-band SAR support within GAMMA Software

Urs Wegmüller, Christophe Magnard, Charles Werner, Gamma Remote Sensing AG

Version 17-Nov-2023

1. INTRODUCTION

In this document the support provided in the GAMMA Software for the processing of data of the Chinese X-band SAR SV2 (SuperView Neo-2, sometimes also named SuperView-2 or Gaojing-2) is summarized.

China Siwei is planning to build 28 RS commercial satellites system before 2025, with 16 high resolution(0.2-0.3m resolution) optical satellites, 4 wide-width (0.7m resolution + 100km swath width) optical satellites and 8 SAR (X-band, 0.5m resolution) satellites to obtain the capacity of high resolution, wide-width, various sensors, fast receiving, and global coverage.

In July 2022, the first two X-band SAR satellites for this constellation were successfully launched with the names SuperView Neo-2 01/02 [https://www.chinasiwei.com/zgswen/Company1/SuperViewconstellation/list/SuperViewconstellation.html].

In Section 2 the importing of the SuperView Neo-2 SAR SLC data is described, followed by an assessment of the data characteristics, in Section 3. In Section 4, the DInSAR processing sequence for a repeat pass interferometric SV2 data pair acquired with a 17-day time interval is presented. In Section 5, a tandem pair consisting of the mono-static reference scene and the corresponding bistatic second scene is interferometrically processed. The main result generated is a terrain height correction relative to a pre-existing DEM.

2. IMPORTING SV2 SLC DATA

2.1. Importing SLC data

SV2 SLC data are provided as a GeoTIFF with meta data in XML format, that can be read / imported using the program ***par_SV2_SLC***.

par_SV2_SLC SV2-03_MONO_KSBJ71_STRIP_004488_W70.6_S17.2_20230505_SLC_HH_L1A_0000129900.tiff SV2-03_MONO_KSBJ71_STRIP_004488_W70.6_S17.2_20230505_SLC_HH_L1A_0000129900.meta.xml 20230505.slc.par 20230505.slc 0

As input, the GeoTIFF and the meta data XML files are indicated. The program generates the SLC binary data file, in SCOMPLEX or FCOMPLEX format, and the related SLC parameter file. The SLC can be visualized using

disSLC 20230505.slc 10612 1 32000 1. .35 0

and the spectrum can be checked using

dismph_fft 20230505.slc 10612 1 0 1. .35 128 3 0 &

The orbit state vectors appear not "noisy" but there is a jump in the correction from positive to negative values. Most likely, the state vectors correspond to post-processed GNSS measurements. Using the program *ORB_filt_spline.py* the state vector quality can be checked / improved.

/bin/cp 20230505.slc.par 20230505.slc.par.orig

ORB_filt_spline.py 20230505.slc.par.orig 20230505.slc.par.tmp --png png_dir --degree 5

The statistics centimeter scale standard deviation of the unfiltered state vector positions from the filtered solution. The generated PNG file with the positional deviations is shown in Figure 1.

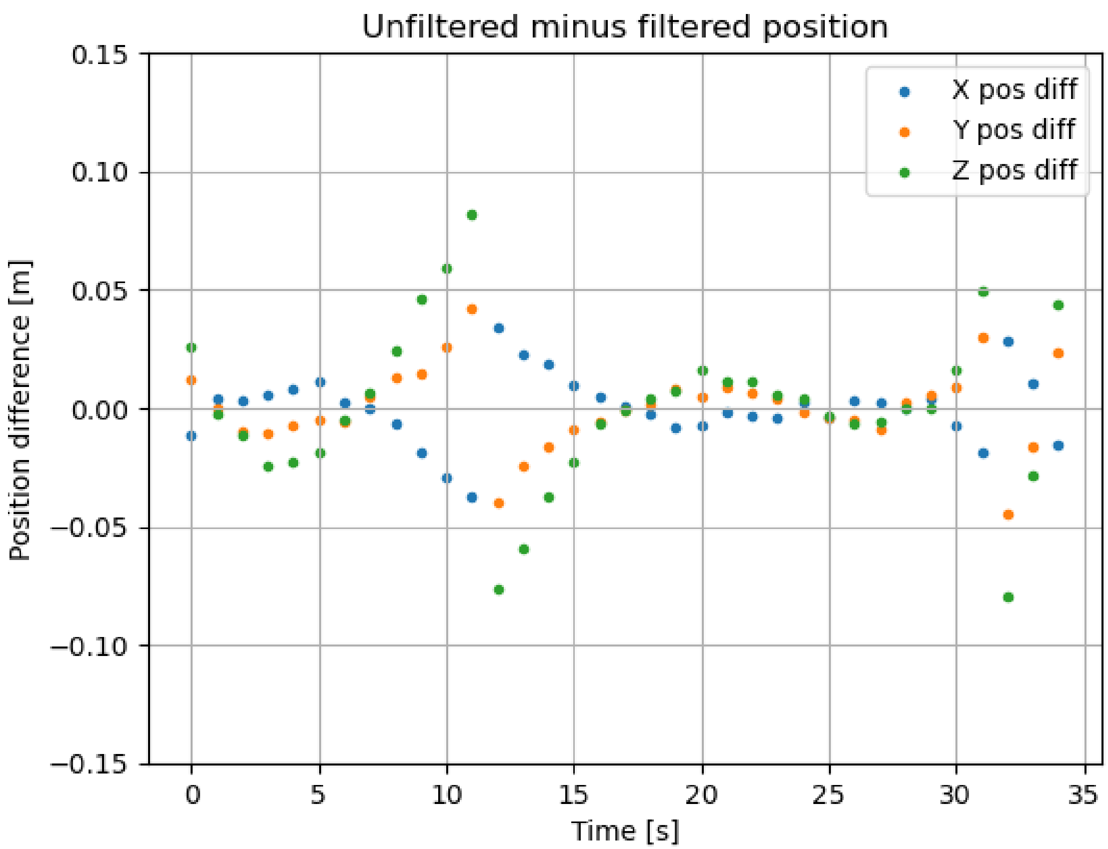

Figure 1 State vector deviations from the filtered solution. There are cm-scale position deviations between the filtered and unfiltered solutions.

We replace the state vectors with filtered state vectors and avoid using the state vectors at the end of the sequence to avoid the outliers. As a result, we obtain the updated 20211221.slc.par.

Using the SLC we generate a backscatter image in slant range geometry using *multi_look* and visualize it using *ras_dB* and *disras*.

A section of the resulting SV2 backscatter image is shown in Figure 2.

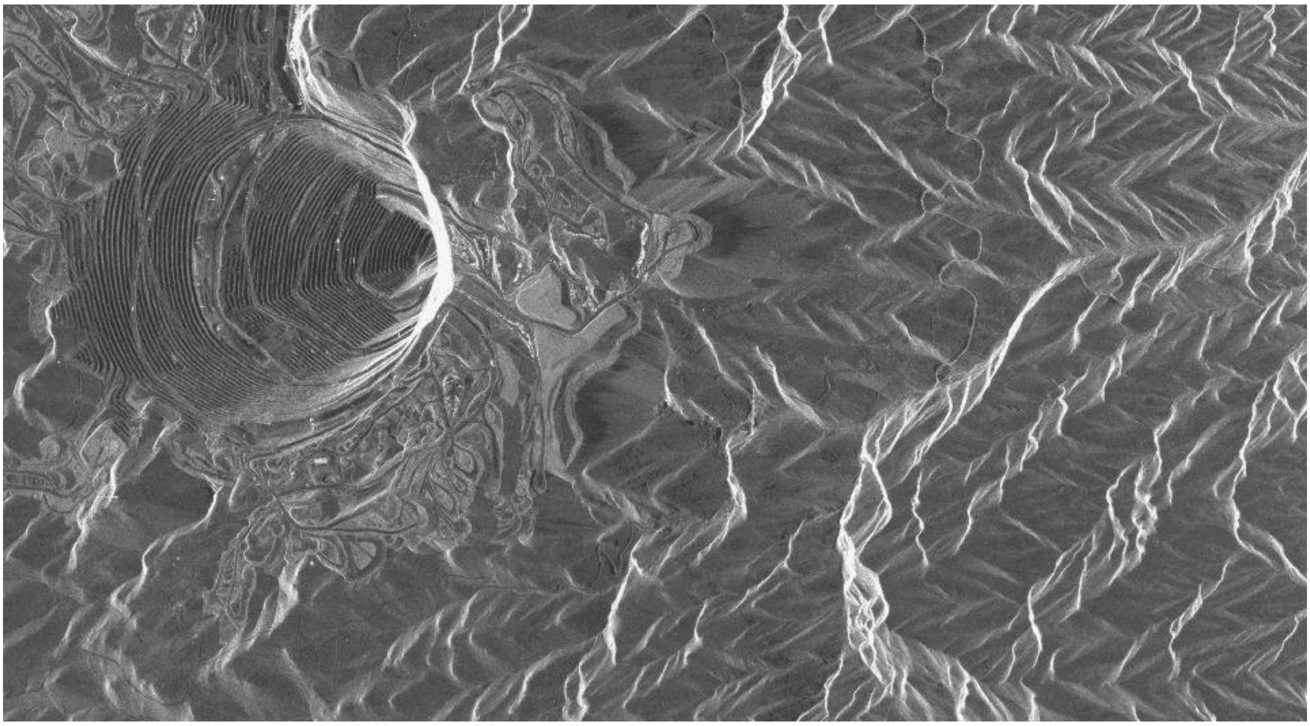

Figure 2 Section of SV2 data (5 x 5 look MLI in slant range geometry).

2.2. Importing detected data in slant range geometry

Not available so far.

2.3. Importing geocoded / georeferenced data

Not available so far.

3. ASSESSMENT OF SOME CHARACTERISTICS OF SV2 STRIPMAP SLC

3.1. Radiometric calibration and estimation of NESZ

We were (so far) not able to conduct an absolute radiometric calibration for SV2 data. Therefore, the data was not radiometrically calibrated in the SLC reading step. In the *multi_look* step we conducted a scaling to bring the backscatter to reasonable values. No validation with different satellite data or targets with known backscatter coefficients was done in our assessment.

Using dark areas (radar shadow and smooth water surfaces) we estimated a Noise Equivalent Sigma Zero value. Provided that we did not apply an accurate radiometric calibration there is a certain uncertainty but sufficient to find that the NESZ value is quite low (< -18 dB).

3.2. Point target characteristics

Considering several small, strong scatterers present in the scene we determined the following point target characteristics (for a Fine-Spotlight mode scene of SV2-04):

slant range resolution (3dB):	0.28 m
azimuth resolution (3dB):	0.39 m
peak_side_lobe_ratio:	< -20 dB

3.3. Geocoding

We generated a multi-look intensity image using 5 range and 5 azimuth looks and conducted a geocoding sequence, using the 1-arc-second Copernicus DEM. As part of the geocoding sequence a refinement was determined based on the offset between a simulated backscatter image (calculated based on the orbit data and the DEM) and the actual SAR backscatter.

The refinement statistics indicate for the offset estimates a very small standard deviation of below 0.2 multi-look pixel in both slant range and azimuth directions. For the data acquired in 2023, the determined range and azimuth offsets were also small (< 2m). A geocoded backscatter image is shown in Figure 3. Because of the mountainous terrain a large fraction of the area is in layover.

3.4. RFI filtering

The data we had available was not affected by Radio-Frequency-Interference (RFI), causing ghost images, and zones with significantly increased noise, etc. So no RFI filtering was necessary.

GAMMA *Remote Sensing AG, Worbstrasse 225, CH-3073 Gümligen, Switzerland*
tel: +41-31-951 70 05, fax: +41-31-951 70 08, email: wegmuller@gamma-rs.ch

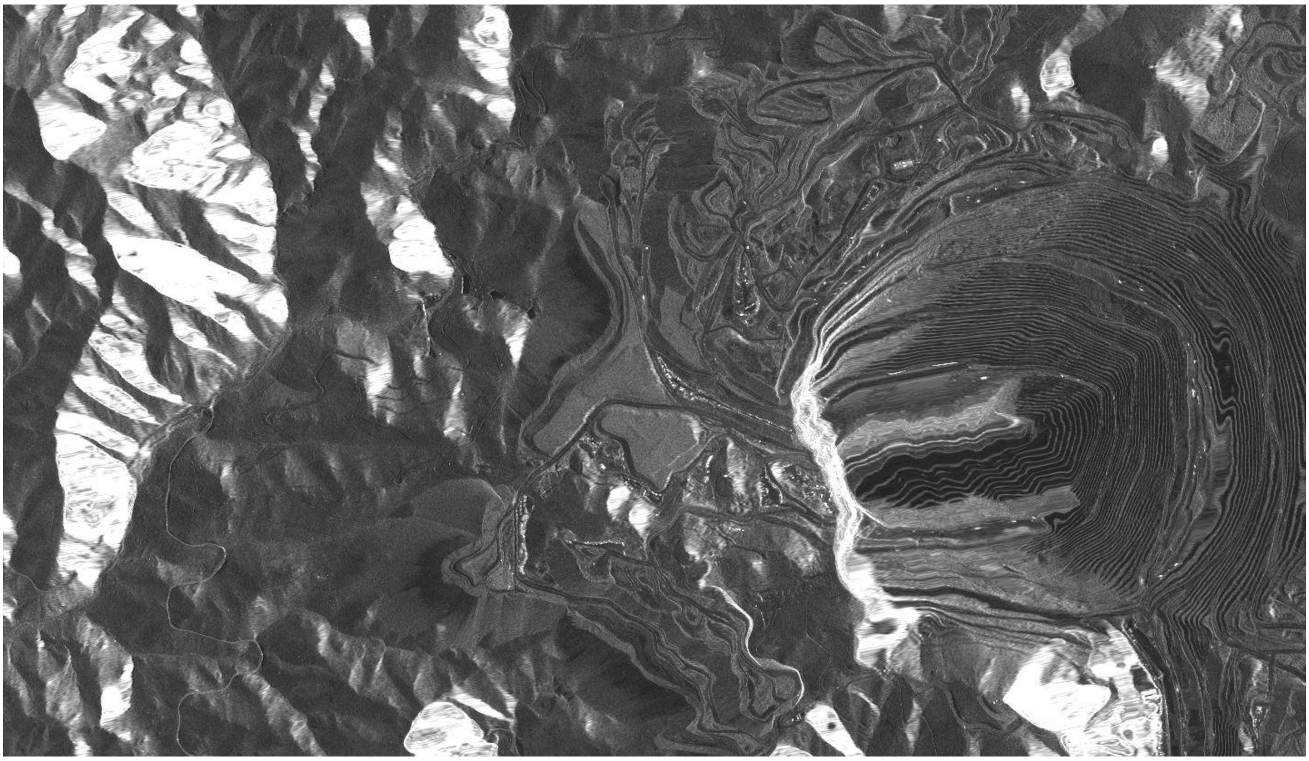

Figure 3 Section of a geocoded SV2 backscatter image over Chile.

4. SV2 REPEAT-PASS DIFFERENTIAL SAR INTERFEROMETRY (DINSAR)

4.1. Processing sequence used and results

We were able to test SV2 differential SAR interferometry using an SV2 pair with 17 days difference and a perpendicular baseline component of about 132m, acquired on 5. and 22. May 2023 over the, Chile.

A flow chart of the processing sequence used is shown in Figure 4. In the following, some of the steps are further discussed.

The two scenes used were acquired by SV2-03 (second scene, 22. May 2023) and SV2-03 (reference scene, 5. May 2023). The importing of the two SLCs is done using the program *par_SV2_SLC*. After the importing we checked and filtered the orbit state vectors.

We selected then the earlier scene as the reference, generated a multi-look intensity image (MLI) with 5 range and 5 azimuth looks, and conducted a geocoding sequence using the Copernicus 30m global DEM. This also included the resampling of the DEM height into the MLI geometry.

Next, we co-registered the second SLC to the reference SLC. In this we used a sequence that also considers the terrain height (using *rdc_trans*). In this a refinement is done using intensity matching, to achieve a co-registration accuracy better than 0.1 SLC pixel.

Then we calculated the orbital and topographic phase (*phase_sim_orb*) and the differential interferogram (*SLC_diff_intf*). The resulting differential interferogram has a high coherence but shows a quite substantial overall phase trend, mainly in the azimuth direction (Figure 5a). We unwrap the differential interferogram (*mcf*), estimate the overall phase trend (*quad_fit*, Figure 5b), and subtract it (*sub_phase*), to get the "detrended" differential interferogram (Figure 5c).

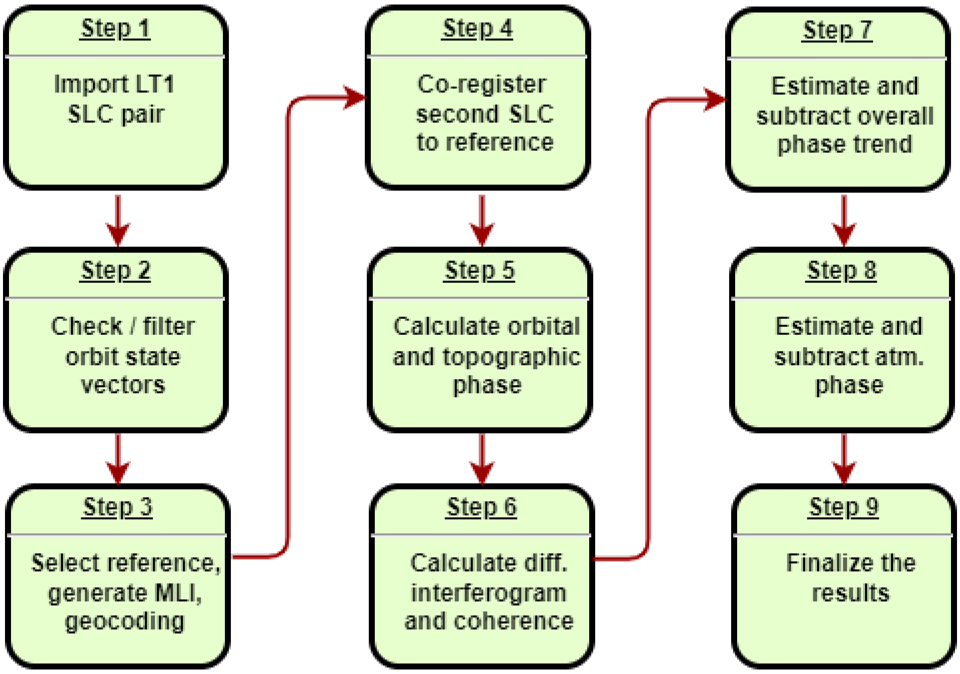

Figure 4 Flowchart of DInSAR processing sequence used.

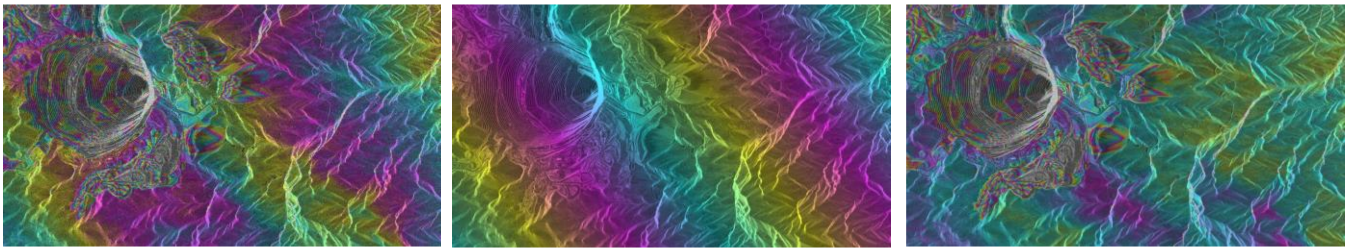

a) differential interferogram b) estimated trend c) detrended interferogram

Figure 5 "Detrending" of SV2 differential interferogram.

Starting from the "detrended" differential interferogram we would normally estimate an atmospheric path delay. In this example this is difficult because of the presence of strong topographic phases in the mining area present in the scene. Distinguishing deformation phase, atmospheric phase and topographic phase with the single differential interferogram cannot be reliably be done. Probably most of the phase is topographic phase (Figure 6), but there is also about significant atmospheric phase present. To identify displacements in the mining area further acquisitions or a current high resolution DEM would be needed.

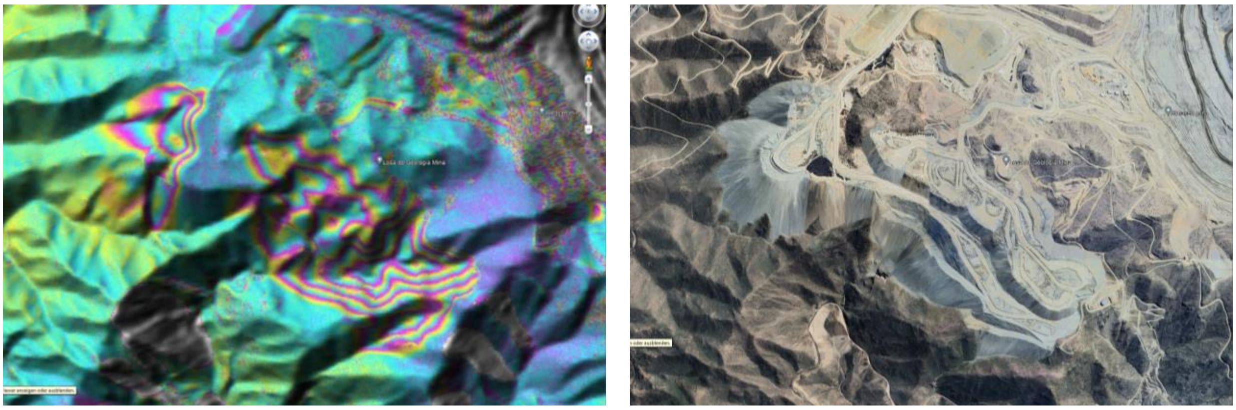

a) differential interferogram b) same area in Google Earth

Figure 6 SV2 differential interferogram. The main phase contribution is topographic phase related to terrain changes from mining activities.

4.2. Discussion

The example investigated clearly confirms that SV2 can be used for repeat-pass SAR interferometry. For the dry rocky area the coherence is mostly very high.

5. SV2 SINGLE-PASS DIFFERENTIAL SAR INTERFEROMETRY (TANDEM-DINSAR)

5.1. RFI filtering

Reading of the bistatic pair is done in the same was as shown in 4.1 using *par_SV2_SLC*. Then we check the xml file to determine which of the two scenes acquired by the SV2-03 and SV2-04 is the active one (it is SV2-04 in this case) and use it as the geometric reference.

Checking the data we see that the bistatic scene received by the SV2-03 shows some anomalies in the near range. Checking the spectrum with dismph_fft shows that this is most likely related to low frequency part of the range spectrum. Applying slight range band-pass filtering

bpf SV2-03_20230131.slc SV2-03_20230131.slc.bpf_filt 23894 0.0 0.4 0.0 0.7 - - - - 0

permits getting rid of this problem. Figure 7 shows for a small section in the near range the original and RFI filtered backscatter image.

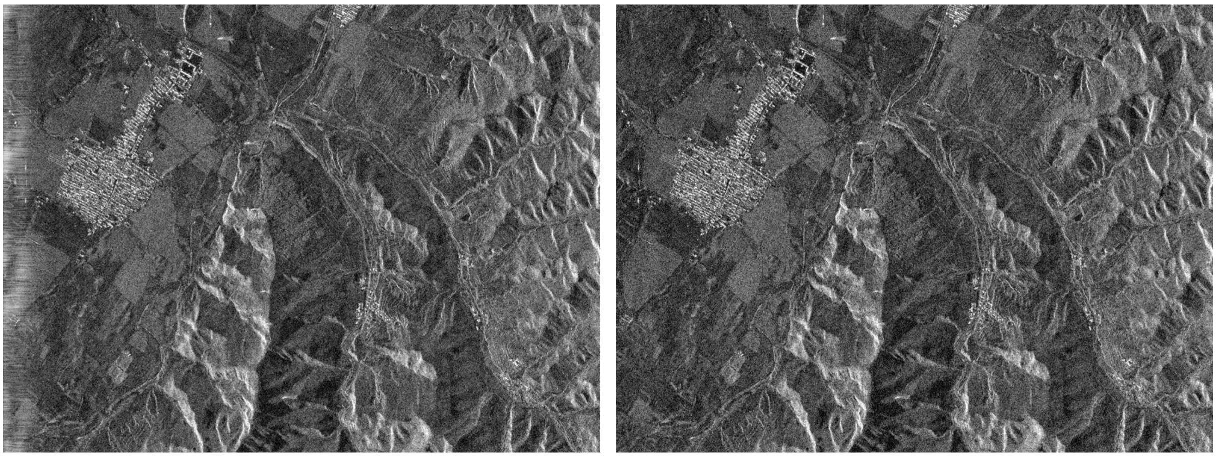

Figure 7 Original (left) and RFI-filtered (right) backscatter image. The anomaly in the near range is removed.

5.1. Processing sequence used

After the launch of SV2-03 and SV2-04 in 2023 the two X-band SAR sensors are operated in a Tandem mode with one sensor transmitting and receiving (monostatic acquisition) and the other one also receiving the signal transmitted by the first (transmitting) sensor (bistatic acquisition). Combining the monostatic and bistatic acquisitions support single-pass interferometry. Single-pass interferometry with a spatial baseline can be used to determine topographic heights. Examples for this are the SRTM DEM that was generated using the single-pass C-band acquisitions and the Copernicus DEM that is uses X-band single-pass acquisitions acquired by the Tandem-X satellite constellation.

For our testing we used a single pass SV2-04/SV2-03 tandem pair acquired with a perpendicular baseline component of about -360m, acquired on 31. Jan. 2023.

A flow chart of the processing sequence used is shown in Figure 8. In the following some of the steps are further discussed.

GAMMA Remote Sensing AG, Worbstrasse 225, CH-3073 Gümligen, Switzerland
tel: +41-31-951 70 05, fax: +41-31-951 70 08, email: wegmuller@gamma-rs.ch

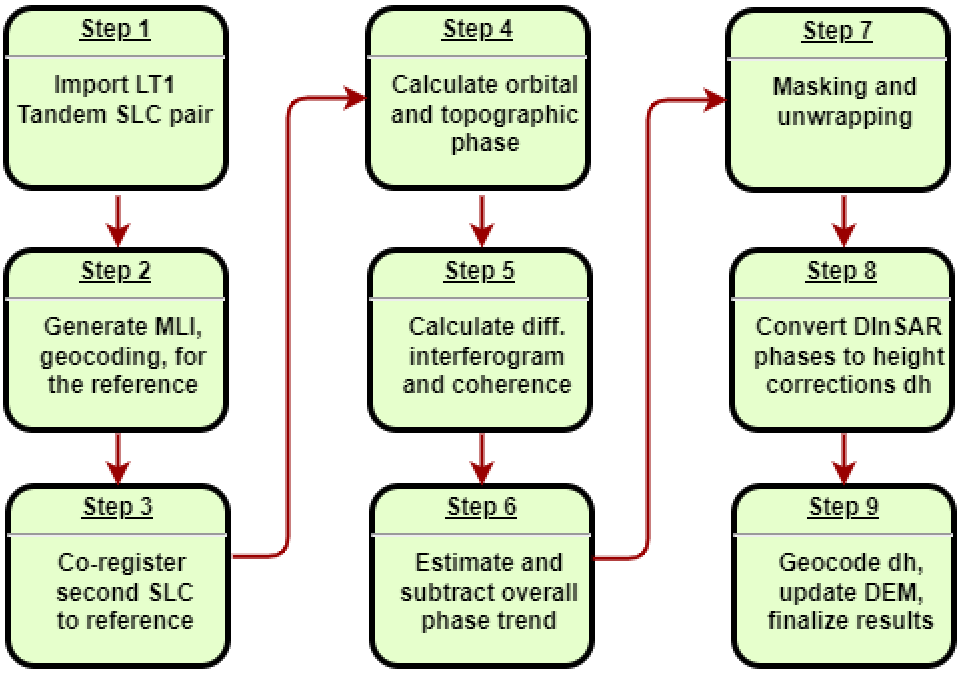

Figure 8 High-level flowchart of DInSAR processing sequence used to update a pre-existing DEM based on a SV2 Tandem pair.

The importing of the scenes is done using the program *par_SV2_SLC*. Importing of the bistatic scene is done in the same way as for the monostatic scene. With the bistatic acquisition, XML files with meta data are provided per data set. In addition, a third XML is provided with a name that includes SV2AB. Among other things this file informs about which one of the two sensors is the monostatic (active) and which one the bistatic (passive) sensor. In our example SV2-04 is the active sensor, so we use SV2-04 as the reference of the single-pass interferometric pair.

As for other SV2 SLC data we recommend to check/filter the orbit state vectors immediately after reading the data (to assure that the filtered state vectors are present e.g. in the MLI parameter file). This checking/filtering is done using the program *ORB_filt_spline.py*. In our example there was for both scenes for one coordinate a saw tooth deviation with a magnitude of about 5cm. We think that this may be related to a quantization issue (not of the state vectors provided with the data but with a previous intermediary element used in the navigation data processing).

The monostatic scene is selected as the reference, a multi-look intensity image (MLI) with 6 range and 4 azimuth looks is generated, and a geocoding sequence using the Copernicus 30m global DEM is conducted. This also included the resampling of the DEM height into the reference MLI geometry.

In the co-registration of the second scene, which is the bistatic acquisition, to the reference, we have to consider that the second scene is not a different monostatic scene but a bistatic scene. For the bistatic acquisition, the two-way slant range is the sum of the slant ranges from the first orbit to the target (r1) and from the target to the second orbit (r2). So the “effective slant range” is (r1+r2)/2 (and not r2. A co-registration procedure using the older version of *rdc_trans* was implemented in *SLC_coreg_tandem.py*. Starting with the Dec. 2023 release, updated versions of *rdc_trans* and *SLC_coreg.py* with a “tandem mode option” will be available in the software.

In the co-registration of a pair with a long spatial baseline, considering the terrain topography effects is relevant. Using a constant height instead of a DEM or using a DEM with significant errors may result in imperfect co-registration. Co-registration errors > 0.2 pixel in slant range result in a reduction of the coherence, errors > 1 pixel may result in a complete decorrelation. Doing the processing without a DEM, assuming a constant height, seems reasonable. A refinement step would then be applied based on an offset field estimated using *offset_pwr_tracking*.

After the co-registration, the simulation of the orbital and topographic phase is done using *phase_sim_orb*. Here it is important that the "single-pass mode" is used. Using the co-registered SLC and the simulated orbital and topographic phase we can then calculate the single-pass differential interferogram (using *SLC_diff_intf*). For a single-pass interferogram there is no temporal decorrelation, so we expect that the coherence is very high. Low coherence is observed for layover and shadow areas, for areas with very low backscatter (e.g. smooth water surfaces and wet snow). Non-overlapping parts of the reflectivity spectra may also reduce the coherence (depending on the perpendicular baseline component) and for areas with significant volume scattering the coherence may also be reduced (by "volume decorrelation"), again depending on the length of the perpendicular baseline component.

For the SV2 single-pass differential interferogram it was necessary to estimate and subtract an overall phase trend (possibly related to orbit errors or processing effects, Figure 9).

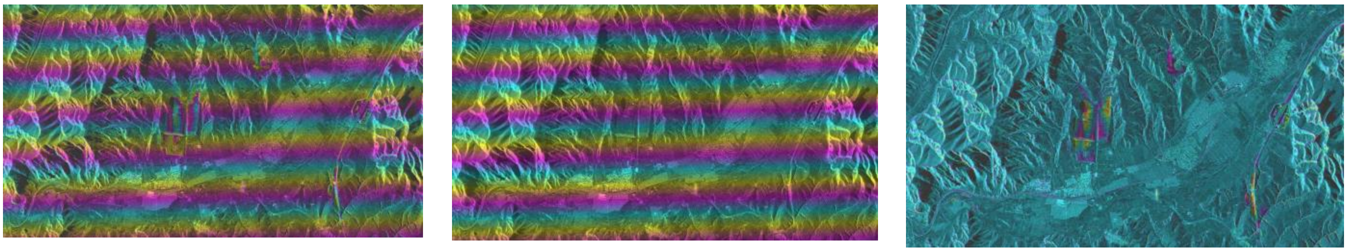

a) differential interferogram b) estimated trend c) detrended interferogram

Figure 9 "Detrending" of SV2 Tandem differential interferogram.

After getting the detrended single-pass differential interferogram, the phase needs to be unwrapped. In layover/shadow areas, and very close to such areas the phase is very noisy. It is recommended to mask layover and shadow areas and as well areas with low coherence. The resulting area can be unwrapped using *mcf*, or if phases are all in the interval (-π,π) using *cpx_to_real*. The phase values can then be converted to height corrections using *dh_map_orb*. With a perpendicular baseline of -360m the phase to height sensitivity of the single-pass DInSAR phase is about 0.133 radian/meter (respectively 7.52 meter/radian). The topographic phases observed (Figure 10) are very plausible, as they are in a mining area.

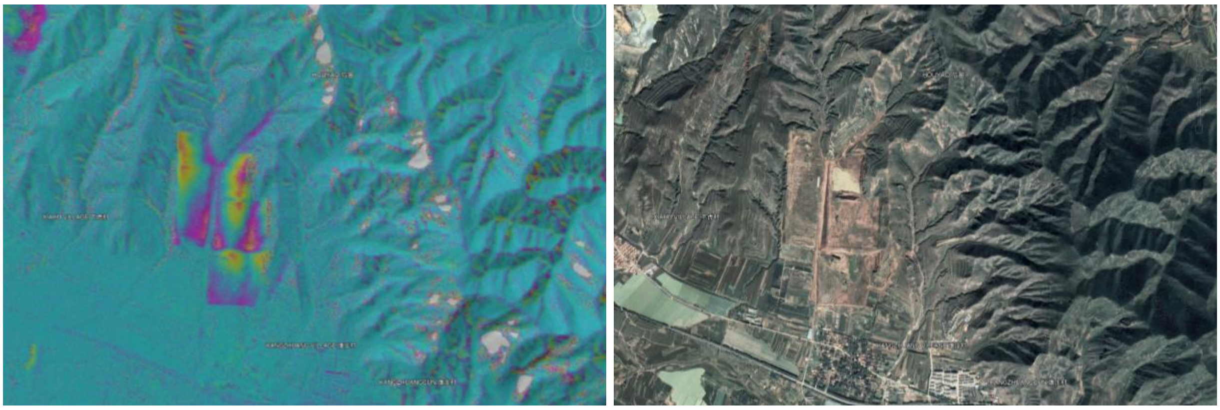

Figure 10 Topographic phases (corresponding to height correction up to about 25m) are located in an area where Google Earth images suggest that terrain changes happened (mining, land fill).

Now the height corrections need to be geocoded from the slant-range MLI geometry to the map geometry. Using the lookup table calculated in the normal geocoding sequence (using the available external DEM, i.e. uncorrected heights) is not precise. The new, corrected DEM heights now available in the slant-range MLI geometry should be used. This is possible using *gc_insar*. The calculated lookup table is in the dimension of the slant-range MLI image and the values correspond to the corresponding locations in the map geometry. A refinement of the lookup table can be done by resampling the MLI to the map geometry and determining offset parameters using a matching procedure of the transformed MLI and the previously geocoded backscatter using the DEM.

5.2 Discussion

The single-pass example investigated clearly confirms the successful operation of the SV2-03/04 as a constellation. The bistatic scene, the related meta data, and the resulting X-band Tandem interferogram are of good quality. The processing sequence confirms that updating of a pre-existing DEM can be achieved.

To achieve a high quality DEMs over an area in a robust manner, it would be necessary to use multiple Tandem pairs including both ascending and descending orbit. With a single orbital direction, the spatial coverage in mountainous areas is limited by layover and shadow effects.

6. ACKNOWLEDGMENT AND COPYRIGHTS

...